International Journal Of
Industrial Electronics Control and Optimization
Print ISSN: 3517-2645
Online ISSN: 3568-2645
Homepage: https://ieco.usb.ac.ir/

Adhesion Force Estimation of Railway Vehicles using Intelligent Square Root Cubature Kalman Filter

Ramazan Havangi
Faculty of Electrical Engineering and Computer, University of Birjand, Iran.
Corresponding author's email: Havangi@Birjand.ac.ir

Article Info

Article type:
Research Article

Article history:
Received: **********
Received in revised form: **********
Accepted: **********
Published online: **********

Keywords: Adhesion force, Square root cubature Kalman filter, Railway vehicles, Differential evolution (DE)

ABSTRACT

Railway traction systems rely on the adhesion force between wheels and rails to effectively transmit mechanical power. Accurate estimation of this force is crucial to avoid wheel slip, improve safety, and enhance traction and braking performance. However, due to the influence of numerous uncertain factors, adhesion force estimation is a complex task. This paper proposes an Intelligent Square Root Cubature Kalman Filter (ISRCKF) for the estimation of wheel–rail adhesion force, without requiring prior knowledge of noise statistics. The proposed method integrates the Differential Evolution (DE) algorithm to adaptively tune the process and measurement noise covariance matrices Q and R, enhancing estimation accuracy and robustness under unknown and time-varying disturbances. In addition, the square-root formulation ensures that all covariance matrices remain positive semi-definite, thereby improving numerical stability. The proposed approach actively contributes to improving traction utilization and reducing wheel wear by minimizing excessive creepage. Simulation results indicate that the proposed ISRCKF achieves a 20% reduction in speed RMSE and a 50% reduction in load torque RMSE compared to the Unscented Kalman Filter (UKF). Additionally, the ISRCKF exhibits a faster convergence rate, enabling rapid stabilization of adhesion force estimates under varying wheel–rail conditions

I. Introduction

Estimating the adhesion conditions at the wheel-rail contact interface during railway operations is a crucial undertaking for the railway industry. The adhesion force encountered in this interface is not only difficult to measure but also influenced by numerous uncertain parameters [1]. Accurately estimating the adhesion force is crucial for understanding the braking and traction capabilities, which play a vital role in performance and safety considerations [2-3]. However, determining the adhesion force is a challenging task due to the simultaneous consideration of various operational and environmental factors, including weather conditions and load conditions [4]. In addition, when the adhesion is underestimated, unexpected occurrences of wear as well as noise at the wheel-rail interface may be detected during operation [4-5]. Researchers focus on estimation of adhesion force.

In the past few years, there have been various proposed models, such as the Kalker model, Oldrich Polach model, and Beam model, aimed at estimating the adhesion force[6-8]. However, these models cannot accurately determine the adhesion characteristics in practical use. Maximum likelihood estimation identifies the adhesion model but is time-consuming and not easy to do on-line [4],[9]. Sliding mode observers estimate adhesion force with a simple structure and strong robustness, but the disadvantage of which is the inevitable chattering phenomenon [10].

A novel approach has been proposed in [11-12] to estimate the adhesion force of the traction AC motor. This approach utilizes the stator voltage, current, and speed, and employs the Extended Kalman filter (EKF) for accurate estimation. Another method is multi-rate EKF state identification to detect slip velocity[13-14]. The Kalman-Bucy filtering technique is employed to estimate the forces causing creep on the rear wheelset of the front bogie. This estimation is based on a non-linear contact mechanics model of the half vehicle [15-16]. To effectively address the wheel slip/slide phenomenon and estimate the adhesion restriction, a multiple version estimation method is utilized. This method involves employing a bank of Kalman filters at specific operation points to accurately identify the adhesion levels [17-19]. Nevertheless, the EKF employs a simplified representation of the machine through the computation of the Jacobian matrix. Unfortunately, this approach not only introduces additional intricacy and hardware implementation challenges but also proves inadequate for highly nonlinear model systems.

In situations where the system exhibits significant nonlinearity, the EKF may not provide sufficiently accurate results, thereby leading to the possibility of divergence. Furthermore, in order to linearize the system and acquire the Jacobian matrices, it is necessary for the system to possess continuous differentiability. Consequently, due to the computational complexity involved in calculating the Jacobian matrices, the EKF incurs substantial computational costs. In order to address these challenges, the unscented Kalman filter (UKF) is utilized to estimate the adhesion force.

The UKF is a recursive linear estimator. In this method, a set of sigma points are used to calculate the mean and the covariance estimation. Computational complexity is reduced when these sigma points are used in the UKF. In [20-21], UKF is used to estimate the adhesion force from traction motor behaviours. Using the traction motor behaviors, UKF is used to calculate the binding force. Under various contact conditions, UKF gave accurate friction estimation, but the estimated friction coefficient is unreliable and also affected by the traction load when it is very low. These issues are the result of inaccurate observations and a flawed system dynamic model. However, it can be challenging to change the UKF parameters in a variety of applications to get the intended performance. Furthermore, the effectiveness of the filter in higher dimensions could be diminished as a consequence of a specific parameter in the UKF becoming negative.

To address UKF drawbacks, a cubature Kalman filter (CKF) is presented [22]. The CKF overcomes the difficulties associated with evaluating the Jacobian matrix, as experienced in the EKF. Moreover, it eliminates the need for parameter tuning, which is necessary in the case of UKF[23-24]. A limitation CKF for estimation of the adhesion force is that a priori statistics of the stochastic errors in both measurement and process models are assumed to be available. It is intractable to obtain an accurate estimation with the unknown statistical characteristics of noise. Therefore, the development and application of CKF method have been limited. However, accurate noise statistics data are difficult to obtain, and they are subject to change over time. Consequently, the set of unknown time-various statistical parameters of noise needs to be simultaneously estimated with the system state and the error covariance. The covariance matrix additionally needs to be symmetric and positive definite in order to carry out an accurate state estimation and set up the convergence condition for CKF. In many instances, the covariance matrix turns negative definite as a result of computational inaccuracy and numerical errors. Recent studies have aimed to enhance the robustness and adaptability of Kalman filter variants in complex railway environments. For example, the STF-SCKF-NE algorithm proposed in [25] addresses nonlinear adhesion estimation but still relies on fixed noise covariance matrices, limiting its adaptability to time-varying conditions. In [26], a high-order Cubature Kalman Filter (CKF) is presented for joint estimation of vehicle dynamics and road adhesion coefficient, offering improved nonlinear performance. However, this approach lacks a mechanism for online noise adaptation, which is critical in practical traction systems.

Furthermore, an Interacting Multiple Model (IMM)-based SRCKF is employed in [27] to increase robustness in vehicle state estimation under dynamic operating scenarios. While this technique improves estimation accuracy, it comes at the cost of increased computational complexity, making real-time implementation more challenging.

In this study, we propose a novel approach based on an Intelligent Square Root Cubature Kalman Filter for estimating the wheel–rail adhesion force. The proposed method models the dynamics of a traction system comprising wheels, gearbox, and motor, with contact dynamics described using the Polach model. Instead of propagating full covariance matrices, our method computes and propagates their Cholesky factors, inherently ensuring positive semi-definiteness and improving numerical stability. Moreover, to overcome the limitations posed by unknown and time-varying noise statistics, we integrate DE algorithm for online optimization of noise covariance matrices. This adaptation enhances estimation robustness under varying operating conditions. The estimated adhesion-creep curve is then used to identify optimal traction operating points. The methodology is evaluated under multiple friction scenarios. The key contributions of this paper are summarized as follows:

1. Numerical Stability: The SRCKF propagates the square root (Cholesky factor) of the covariance matrix rather than the covariance matrix itself, ensuring numerical stability and maintaining positive semi-definiteness throughout the filtering process. This property is critical in long-term real-time applications, preventing filter divergence and improving robustness.

2. Adaptive Noise Covariance Tuning: Our method enhances the SRCKF by integrating a Differential Evolution (DE) algorithm that adaptively tunes the process and measurement noise covariance matrices online. This adaptive feature addresses the practical challenge of unknown and time-varying noise statistics in railway environments, improving estimation accuracy and robustness without increasing algorithmic complexity.

3. Computational Efficiency: Compared to more complex filtering techniques such as interacting multiple model filters or particle filters, the SRCKF combined with DE maintains a low computational burden, making it suitable for embedded systems with limited processing capabilities.

4. Improved Nonlinear Estimation: The SRCKF uses a third-degree spherical-radial cubature rule for Gaussian

$$\begin{bmatrix} \dot{i}_{s\alpha} \\ \dot{i}_{s\beta} \\ \dot{\varphi}_{r\alpha} \\ \dot{\varphi}_{r\beta} \\ \dot{w}_m \\ \dot{T}_L \end{bmatrix} = \begin{bmatrix} -(\frac{R_s}{L_\sigma} + \frac{R_r L_m^2}{L_r^2 L_\sigma}) & 0 & \frac{R_r L_m}{L_r^2 L_\sigma} & \frac{L_m}{L_r L_\sigma}\rho_p\omega_m & 0 & 0 \\ 0 & (\frac{R_s}{L_\sigma} + \frac{R_r L_m^2}{L_r^2 L_\sigma}) & -\frac{L_m}{L_r L_\sigma}\rho_p\omega_m & \frac{R_r L_m}{L_r^2 L_\sigma} & 0 & 0 \\ \frac{R_r}{L_r}L_m & 0 & -\frac{R_r}{L_r} & -\rho_p\omega_m & 0 & 0 \\ 0 & \frac{R_r}{L_r}L_m & \rho_p\omega_m & -\frac{R_r}{L_r} & 0 & 0 \\ -\frac{3}{2}\frac{\rho_p}{J_t}\frac{L_m}{L_r}\varphi_{r\beta} & \frac{3}{2}\frac{\rho_p}{J_t}\frac{L_m}{L_r}\varphi_{r\alpha} & 0 & 0 & 1 & -\frac{1}{J_t} \\ 0 & 0 & 0 & 0 & 0 & 1 \end{bmatrix} \begin{bmatrix} i_{s\alpha} \\ i_{s\beta} \\ \varphi_{r\alpha} \\ \varphi_{r\beta} \\ w_m \\ T_L \end{bmatrix} + \begin{bmatrix} 0 & \frac{1}{L_\sigma} \\ \frac{1}{L_\sigma} & 0 \\ 0 & 0 \\ 0 & 0 \\ 0 & 0 \\ 0 & 0 \end{bmatrix} \begin{bmatrix} v_{s\alpha} \\ v_{s\beta} \end{bmatrix} \quad (11)$$

integrals, providing higher accuracy than EKF and avoiding the parameter tuning difficulties of the UKF.

The remainder of this paper is organized as follows: Section 2 presents the problem formulation. Section 3 describes the proposed ISRCKF-based estimation methodology. Section 4 discusses the experimental results. Finally, Section 5 concludes the paper.

II. Modelling of System

The wheel-rail system and the wheel-rail adhesion force dynamic model are explained in this section. The model comprises three essential components: a traction motor, wheels and rails, and a gearbox[2]. The main purpose of the traction system is to transfer the rotational force generated by the traction motor to the wheelset via the gearbox, enabling the wheels to rotate at a speed known as vd. It is important to note that when traction is engaged, the wheel speed v_c is consistently higher than v_t. The difference in speed between the vehicle and the wheels during traction operation is commonly referred to as vs. The locomotive is propelled in a forward direction due to the adhesion force Fμ, which arises from the creeping phenomenon occurring between the train's wheel and the railway track.

A. Model of Adherence Force

An adhesion force occurs between the rails and wheels only when there is a certain amount of velocity difference. This velocity difference, known as slip velocity, is defined as [1-2]:

$$v_s = v_c - v_t \quad (1)$$

A term slip instead of the slip velocity is used more often. The slip ξ is defined as follows:

$$\xi = \frac{v_c - v_t}{v_t} \quad (2)$$

The adhesion force Fμ is modelled in this paper using Polach's technique [4-5]:

$$F\mu = \frac{2F_N\mu}{\pi}\left(\frac{k_A\epsilon}{1+(k_A\epsilon)^2} + \arctan(k_S\epsilon)\right),\ k_S \le k_A \le 1 \quad (3)$$

where μ represents the coefficient of adhesion, and F_N denotes the normal force exerted on the wheel. In a static state, the F_N is a constant value and in a dynamic state the F_N changes. In the case of the longitudinal force ϵ, the following relation holds [6]:

$$\epsilon = \frac{G\pi abC_{11}}{4F_N\mu}\xi \quad (4)$$

where G is the modulus of rigidity of the wheel and rail, ξ is the creepage between the wheel and rail. Then coefficient μ depends on the slip velocity (ξv_t) and is as follows [8]:

$$\mu = \mu_0((1-D)e^{-B\xi V} + D) \quad (6)$$

where D and B represent reduction factors associated with varying friction coefficients.

B. Modelling of Traction System

The present system utilizes an AC induction motor and a gearbox to facilitate the movement of a wheel set comprising two wheels. The interaction between the wheels and the rail generates creep forces, enabling the railway vehicle to propel forward. The system's motion is governed by dynamic formulae, as outlined in [5-6].

$$\frac{d\omega_m}{dt} = \frac{T_m - T_L}{J_{eqv}} \quad (7)$$

$$\omega_c = \frac{\omega_m}{n_i} \quad (8)$$

The given equation represents the relationship between various parameters in a mechanical system. In this equation, ω_c refers to the angular velocity of the wheel, ω_m represents the angular velocity of the motor, ni signifies the

gear reduction ratio, T_m denotes the torque generated by the motor, and T_L and Jeqv correspond to the load torque and the equivalent moment of inertia, respectively. These variables are interconnected as described in a scholarly reference [2-3].

$$T_L = \frac{2rF_a}{n_i} \tag{9}$$

$$J_{eqv} = J_m + \frac{J_g + J_x + J_{wR} + J_{wL}}{n_i^2} \tag{10}$$

We have several inertial moments to consider. These moments are represented by J_g, for the gearbox, $J_x$for the wheelset axle, J_{wR} for the right wheel, and J_{wL} for the left wheel. Additionally, we have F_a, which signifies the adhesion force exerted by a single wheel. With two measurement-ready input variables and three state variables, a system of fifth-order differential equations can accurately describe an induction motor as Eq.(11).

The measurement of the model can be written as:

$$z = \begin{bmatrix} i_{s\alpha} \\ i_{s\beta} \end{bmatrix} \tag{12}$$

where ρ_p is the pole pairs, J_t is the total inertia of IM and load, R_s is the stator resistance and L_s is the stator inductance, R_r *is* the rotor resistance and L_r is the rotor inductance, $L_\sigma = \sigma L_s$ is the stator transient inductance($\sigma = 1 - \frac{L_m^2}{L_r L_s}$), *Lm* is the mutual inductance, $v_{s\alpha}$ and $v_{s\beta}$ are the measured stator stationary axis components of stator voltages.

III. Estimation of the Wheel-Rail Adhesion Force using Intelligent SRCKF

The design phase of the proposed adhesion force estimator is detailed in this section. The procedure begins with the estimation of the load torque using a traction motor load torque estimator. The estimated load torque is subsequently utilized to compute the wheel–rail adhesion force. In this study, a sixth-order rotor flux-based induction motor (IM) model is adopted and integrated into the framework of the ISRCKF to enable accurate estimation of various internal states of the motor. To implement the ISRCKF, the continuous-time state-space model of the system is formulated as

$$\dot{X} = f(X) + \omega$$

where X is the state vector and ω is the process noise. This continuous-time model is discretised using a sampling period T, resulting in a discrete-time model suitable for real-time implementation:

$$X_k = (I + A^*T)X_{k-1} + GTu_k = A(X_{k-1})X_{k-1} + GTu_k$$

where T is the sampling period. The proposed discrete-time IM model, expressed in the stator stationary reference frame and extended to accommodate the estimation algorithm, is presented in Equation (13). The matrices and vectors comprising this extended model are defined to include mechanical dynamics, electromagnetic torque generation, and rotor flux evolution, all of which are crucial for accurately estimating the load torque and consequently the adhesion force.

$$\begin{aligned} X_k &= A(X_{k-1})X_{k-1} + Bu_k + w_{k-1} \\ z_k &= h(X_k) + v_k = HX_k + v_k \end{aligned} \tag{13}$$

$$\underbrace{\begin{bmatrix} i_{s\alpha}(k) \\ i_{s\beta}(k) \\ \varphi_{r\alpha}(k) \\ \varphi_{r\beta}(k) \\ w_m(k) \\ T_L(k) \end{bmatrix}}_{X_k} = \underbrace{\begin{bmatrix} 1-(R_s+\frac{R_r L_m^2}{L_r^2})\frac{T}{L_\sigma} & 0 & \frac{R_r L_m}{L_r^2 L_\sigma}T_2 & \frac{L_m}{L_r L_\sigma}\rho_p T\omega_m(k-1) & 0 & 0 \\ 0 & 1-(R_s+\frac{R_r L_m^2}{L_r^2})\frac{T}{L_\sigma} & -\frac{L_m}{L_r L_\sigma}\rho_p T\omega_m(k-1) & \frac{R_r L_m}{L_r^2 L_\sigma}T & 0 & 0 \\ \frac{R_r}{L_r}L_m T & 0 & 1-\frac{R_r}{L_r}T & -\rho_p T\omega_m(k-1) & 0 & 0 \\ 0 & \frac{R_r}{L_r}L_m T & \rho_p T\omega_m(k-1) & 1-\frac{R_r}{L_r}T & 0 & 0 \\ -\frac{3}{2}\frac{\rho_p}{J_t}\frac{L_m}{L_r}T\varphi_{r\beta}(k-1) & \frac{3}{2}\frac{\rho_p}{J_t}\frac{L_m}{L_r}T\varphi_{r\alpha}(k-1) & 0 & 0 & 1 & -c_8 \\ 0 & 0 & 0 & 0 & 0 & 1 \end{bmatrix}}_{A(X_{k-1})} \underbrace{\begin{bmatrix} i_{s\alpha}(k-1) \\ i_{s\beta}(k-1) \\ \varphi_{r\alpha}(k-1) \\ \varphi_{r\beta}(k-1) \\ w_m(k-1) \\ T_L(k-1) \end{bmatrix}}_{X_{k-1}} \quad (14)$$

$$+ \underbrace{\begin{bmatrix} \frac{T}{L_\sigma} & 0 & 0 & 0 & 0 & 0 \\ 0 & \frac{T}{L_\sigma} & 0 & 0 & 0 & 0 \end{bmatrix}^T}_{B} \underbrace{\begin{bmatrix} v_{s\alpha}(k) \\ v_{s\beta}(k) \end{bmatrix}}_{u_k} + w_{k-1}$$

$$\underbrace{\begin{bmatrix} i_{s\alpha}(k) \\ i_{s\beta}(k) \end{bmatrix}}_{Z_k} = \underbrace{\begin{bmatrix} 1 & 0 & 0 & 0 & 0 & 0 \\ 0 & 1 & 0 & 0 & 0 & 0 \end{bmatrix}}_{H} X_k + v_k$$

where X_k is the state vector at time step k, u_k is the input (control) vector at time step k, w_k is the process noise vector at time step k, z_k is the measurement vector at time step k, v_k is the measurement noise vector at time step k. Assume at time k-1, $s_{K-1|k-1}$ is the square root of $P_{K-1|k-1}$, the current state cubature points are computed as follows:

$$\chi^i_{k-1|k-1} = s_{k-1|k-1} I(i) + \hat{x}_{k-1|k-1} \qquad i = 1,...2n \quad (15)$$

where $P_{K-1|k-1}$ represents the state estimation error covariance matrix at time step k-1, $I(i)$ is as

$$I(i) = \begin{cases} \sqrt{n}1_i & \text{i=1,...,n} \\ -\sqrt{n}1_{i-n} & i = n+1,...,2n \end{cases} \quad (16)$$

$$P_{K-1|k-1} = s_{K-1|k-1} s^T_{K-1|k-1}$$

where 1_i is the i-th column of the identity matrix I. The cubature points are then transmitted into the state equation: $\chi^{i*}_{k|k-1} = f(\chi^i_{k-1|k-1})$

The predicted mean $\hat{x}_{k|k-1}$ and square root of the covariance matrix $S_{k|k-1}$ are calculated as:

$$\hat{x}_{k|k-1} = \frac{1}{2n}\sum_{i=1}^{2n} \chi^{i*}_{k|k-1} \quad (17)$$

$$s_{k|k-1} = \text{Tria}\left\{X_{k|k-1}, \sqrt{Q_k}\right\} \quad (18)$$

where $X_{k|k-1}$ is:

$$X_{k|k-1} = \frac{1}{\sqrt{2n_x}} \left[\chi^{1*}_{k|k-1} - \hat{x}_{k|k-1} \quad \chi^{2*}_{k|k-1} - \hat{x}_{k|k-1} \quad \cdots \quad \chi^{2n*}_{k|k-1,} - \hat{x}_{k|k-1}\right] \quad (19)$$

In Equations (18), (23), and (27), the operator Tria() denotes the upper triangular matrix obtained via the QR decomposition of the input matrix. This operation is commonly used in square root filtering to preserve the numerical stability and ensure positive semi-definiteness of the covariance matrices. Formally, for a matrix MMM*, we compute* [Q,R]=qr(M)*, and define:*

Tria(M)≜R

where R *is an upper triangular matrix.* We have updated the equations accordingly and clarified this definition in the main text. When measurement is revisited, the cubature point set is calculated as follows:

$$\chi^i_{k|k-1} = s_{k|k-1} I(i) + \hat{x}_{k|k-1} \qquad i = 1,...2n \quad (20)$$

the transformed cubature points are transmitted in measurement equation:

$$\chi^{i**}_{k|k-1} = h(\chi^{i}_{k|k-1}) \tag{21}$$

The mean values and square-root of the covariance matrix of predicted measurement points are estimated:

$$\hat{z}_{k|k-1} = \frac{1}{2n}\sum_{i=0}^{2n} \chi^{**i}_{k|k-1} \tag{22}$$

$$S_{zz,k|k-1} = \mathrm{Tria}\left\{Z_{K|k-1}, S_R\right\} \tag{23}$$

where $Z_{K|k-1}$ is as:

$$Z_{k|k-1} = \frac{1}{\sqrt{2n}} \left[\chi^{1**}_{k|k-1} - \hat{z}_{k|k-1} \quad \chi^{2**}_{k|k-1} - \hat{z}_{k|k-1} \quad \cdots \quad \chi^{2n**}_{k|k-1} - \hat{z}_{k|k-1}\right]$$

$$S_{xz,k|k-1} = X_{k|k-1} Z^{T}_{k|k-1} \tag{24}$$

$$X_{k|k-1} = \frac{1}{\sqrt{2n_x}} \left[\chi^{1}_{k|k-1} - \hat{x}_{k|k-1} \quad \chi^{2}_{k|k-1} - \hat{x}_{k|k-1} \quad \cdots \quad \chi^{2n}_{k|k-1,} - \hat{x}_{k|k-1}\right] \tag{25}$$

The updated state $\hat{x}_{k|k}$ and the square-root of covariance $S_{k|k}$ are obtained as follows:

$$\hat{x}_{k|k} = \hat{x}_{k|k-1} + K_k(z_k - \hat{z}_{k|k-1}) \tag{26}$$

$$S_{k|k} = Tria([X_{k|k-1} - K_k Y_{k|k-1}, K_k\sqrt{R_k}]) \tag{27}$$

where K_k is as:

$$K_k = (S_{xz,k|k-1} / S^{T}_{zz,k|k-1}) / S_{zz,k|k-1} \tag{28}$$

To determine the approximate adhesion force, one can employ the estimated load torque information by performing the following calculation:

$$\hat{T}_L = \frac{2r}{n_i}\hat{F}_a \tag{29}$$

While the square-root cubature Kalman filter (SRCKF) provides a computationally efficient and stable framework for nonlinear estimation, its conventional form assumes prior knowledge of noise statistics (Q and R), which is often impractical in railway applications. Reconsidering the equations of $S_{k|k-1}$ and $S_{k|k}$ in (18) and (28), respectively, it can be concluded that the process covariance matrices Q_k and measurement covariance matrices R_k have a critical effect on their values. As a result, the choice of elements of Q_k and R_k is important in the design of SRCKF since it effects the convergence, performance, and stability of the system. However, obtaining precise noise statistics can be a challenging task, as these statistics can vary with time. In previous studies, researchers have manually adjusted these matrices through trial and error, which is a time-consuming process [26]. To overcome this challenge and eliminate the need for trial and error methods, this paper proposes considering the covariance matrices as adjustable parameters. Our Intelligent SRCKF (ISRCKF) addresses this limitation by integrating a differential evolution algorithm to adaptively tune Q and R. This hybridization retains the numerical stability of SRCKF while adding robustness against uncertain and time-varying noise conditions. The DE optimization ensures that the filter dynamically adjusts to real-world operational challenges, such as varying adhesion coefficients and sensor inaccuracies, without requiring offline calibration. Compared to recent adaptive filters, the ISRCKF achieves comparable accuracy with lower computational complexity.

In proposed method, an alternative for the tuning and optimization of Q_k and R_k based on the DE algorithm is proposed. In this method, set the Q_k and R_k dimensions as 6 × 6 and 2 × 2, which are assumed as:

$$Q = \begin{bmatrix} q_1 & 0 & 0 & 0 & 0 & 0 \\ 0 & q_2 & 0 & 0 & 0 & 0 \\ 0 & 0 & q_3 & 0 & 0 & 0 \\ 0 & 0 & 0 & q_4 & 0 & 0 \\ 0 & 0 & 0 & 0 & q_5 & 0 \\ 0 & 0 & 0 & 0 & 0 & q_6 \end{bmatrix}$$

$$R = \begin{bmatrix} r_1 & 0 \\ 0 & r_2 \end{bmatrix}$$

The aim is to enhance the covariance matrices by modifying the components of Q_k and R_k according to a fitness function. The fitness function serves to minimize the disparity between the estimated and measured values of the stator current.

$$J = \frac{1}{N}\sum_{k=0}^{N}\left[(i_{s\alpha}(k) - \hat{i}_{s\alpha}(k))^2 + (i_{s\beta}(k) - \hat{i}_{s\beta}(k))^2\right] \tag{30}$$

where N represents the number of samples considered. The variable $i_s$denotes the actual stator current, while , $\hat{\imath}_s$ represents the estimated stator current and $\| \|_2$ is the Euclidean distance. Stator current is typically measured using current sensors, and a smaller disparity between the estimated current and its measurement signifies a more precise estimation of the speed of the induction motor.

Suppose $C^k = [c^k_1 \quad \cdots \quad c^k_n]^T$ represents the current population of DE at iteration k, which $c^k_i = \{q^k_{i1} \quad q^k_{i2} \quad q^k_{i3} \quad q^k_{i4} \quad q^k_{i5} \quad q^k_{i6} \quad r^k_{i1} \quad r^k_{i2}\}$ is each candidate solution to the problem of optimization at iteration k. To generate a new population, the crossover, mutation, and selection operators are applied. The crossover and mutation operators are used to generate the trial vectors. A critical stage in the DE process is the creation of the trial

vector. To select the best trial vector, selection operator is used in the next generation. In the suggested approach, the DE mutation operator creates a trail vector for each member of the current population. For each c_i^k in the population, trail vector υ_i^k is generated as follows:

$$\upsilon_i^k = c_i^k + B(c_i^{k,gbest} - c_i^k) \quad (31)$$

vector to be perturbed at iteration k, $c_i^{k,gbest}$ is the target vector in the present population with the smallest value of the objective function. A crossover mechanism is used to increase the diversity of the new population of vectors. The crossover operation is applied to every pair of the target vector c_i^k and its corresponding mutant vector υ_i^k to generate a trial vector $c_i'^k$. The binomial crossover stands as the most frequently utilized crossover method in DE, and it is precisely defined as follows:

$$c_i'^k = \begin{cases} \upsilon_i^k & \text{if } j \in J \\ c_i^k & \text{otherwise} \end{cases} \quad (32)$$

where J is the set of crossover points. Following the crossover, to obtain the fitness function, the trial vectors are evaluated and selection operations are performed. The value of fitness function of each trial vector $J(c_i'^k)$ is compared with its corresponding target vector $J(c_i^k)$. In order to determine whether the trial vector $c_i'^k$ should be included in the next generation $k+1$, it is compared to c_t^k. If the trial vector $c_i'^k$ produces a superior result for the objective function compared to c_t^k will be replaced by $c_i'^k$ in the upcoming generation. Alternatively, if the previous value c_t^k proves to be more favorable, it will be retained for the subsequent generation.

$$c_t^{k+1} = \begin{cases} c_i'^k & \text{if } J(c_i'^k) < J(c_t^k) \\ c_t^k & \text{otherwise} \end{cases} \quad (33)$$

The process of mutation, selection and crossover is repeated after the new population is propagated until the ideal state is reached. When the best fitness value hits a predetermined value, the iteration is terminated. Based on fitness function values, DE optimizes the unknown parameters of Q_k and R_k by updating the particle solutions to provide particles better sets. The new solutions and updated Q_k and R_k are then used for the adaptation of SRCKF for the next iteration until a predetermined number of iterations has been achieved. Subsequently, the most favorable values of Q_k and R_k are acquired. Ultimately, the optimized values of Q_k and R_k are incorporated into the online running SRCKF estimator. It is important to highlight that the intelligent SRCKF needs to be executed multiple times to enable the fine-tuning of the Q_k and R_k parameters based on each individual measurement.

Algorithm 2. Intelligent SRCKF

1: Initialize the particles consisting of the components from Q and R

2: **Iterate the following steps:**

3: Reconstruct Q and R

4: Run SRCKF

5: Evaluate the fitness function particles

7: Update the velocities and positions of the particles using Equations (28) to (29).

9: **Continue until reaching the maximum iteration**

10: Output the optimal particles for reconstructing the matrices Q and R.

After a predetermined number of iterations of the DE algorithm, we are able to acquire the optimal parameter values for the diagonal elements of matrices Q and R. Subsequently, these optimal values are incorporated into the proposed method, resulting in the estimation of the state variables. The intelligent SRCKF is developed in Algorithm 2 by leveraging the principles of the SRCKF and DE.

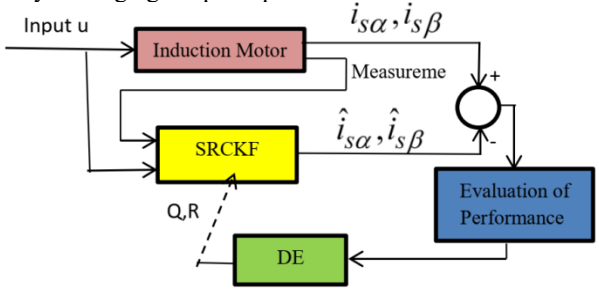

Fig. 1. Block diagram of Intelligent SRCKF

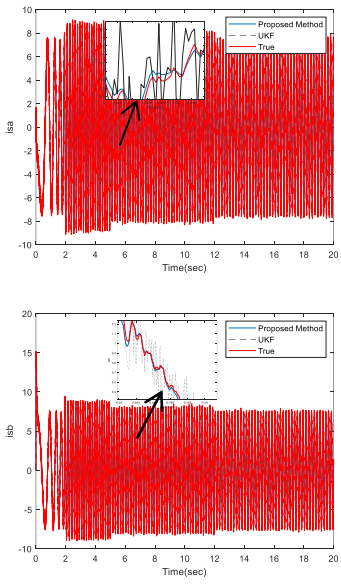

Fig. 2. Estimated currents

IV. Result

In this section, the effectiveness of the proposed approach for adhesion force is evaluated and compares with UKF.

TABLE I Parameters of the traction system employed

Table I. parameters of the IM									
$N_m(r/\min)$	$\tau_i(Nm)$	ρ_p	$R_s(\Omega)$	$R_r(\Omega)$	$L_s(H)$	$L_r(H)$	$L_m(H)$	$J_i(kg.m^2)$	$B_i(nm/rad/s)$
950	22	2	3.03	2.5	0.14	0.15	0.135	0.055	0.001

Table I presents the parameters pertaining to the traction system employed in the simulation. The covariance matrices used in methods are considered as:

$$Q = diag\{10^{-8},10^{-8},10^{-8},10^{-8},10^{-8},10^{-8}\}$$
$$R = diag\{10^{-1},10^{-1}\}$$

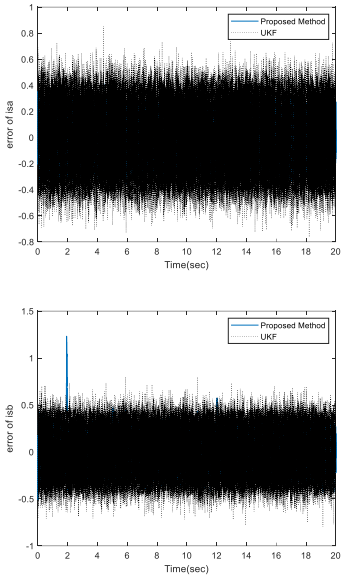

Fig. 3. Current errors

In all conducted experiments, the sampling time was set to *T=0.0001s* in all conducted experiments to ensure accurate tracking of the high-frequency dynamics of the induction motor. This fine resolution is particularly important for capturing the rapid changes in stator currents and rotor flux, and for maintaining numerical stability in the Euler-discretized model used by the SRCKF algorithm. Additionally, the initial conditions for all estimated states in both algorithms were assumed to be zero. The parameters used in these experiments include the semi-axes of the contact ellipse (a = 1.5 × 10-3 m, b = 7.5 × 10-3 m), the normal force at the wheel-rail contact (FN = 50 kN), the longitudinal Kalker's coefficient (C11 = 4.12), and the shear modulus (G = 8.4 × 1010 N/m2). Fig.2 and 3 depict the trajectory of the estimated motor currents and current errors, respectively, using both the suggested technique and UKF. Fig.4 and 5 exhibit the path traced by the estimated rotor fluxes and the corresponding flux errors, respectively.

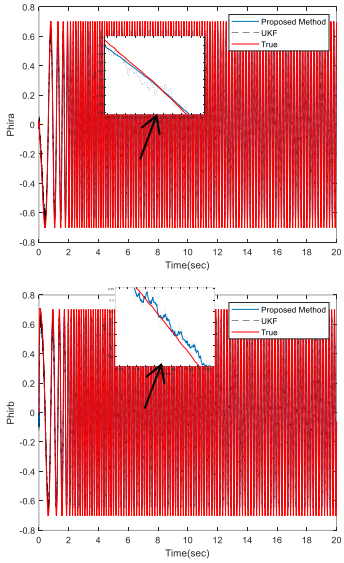

Fig. 4. Estimated fluxes

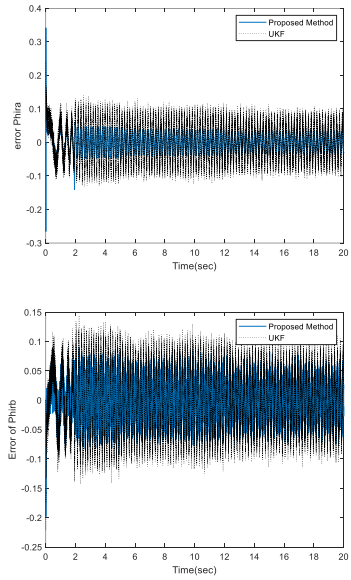

Fig. 5. Flux errors

Fig.6 illustrates the path of both the real and predicted motor speed, along with the speed error. The sudden error spikes observed in the standard Kalman filter at approximately 2 and 5 seconds (Fig. 6) correspond to abrupt changes in the adhesion force, likely caused by rapid variations in slip or external disturbances. During these intervals, the fixed noise covariance matrices used by the standard filter do not accurately capture the system's stochastic behavior, leading to a temporary degradation in

estimation accuracy. The proposed method overcomes this limitation by adaptively updating the noise statistics, thereby maintaining robust performance even under sudden dynamic changes. Extensive evidence confirms that the estimator swiftly converges and accurately follows the speed trajectory, maintaining an impressively minimal margin of error. On the other hand, Fig.7 exhibits the path of the estimated load torque and the associated load torque errors.

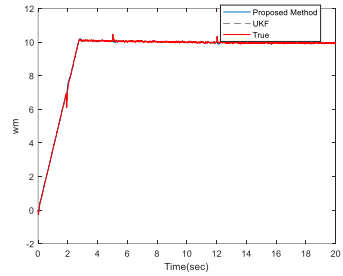

(a)

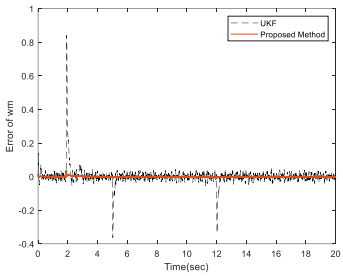

(b)

Fig. 6. a) True and estimated motor speed b) Speed error

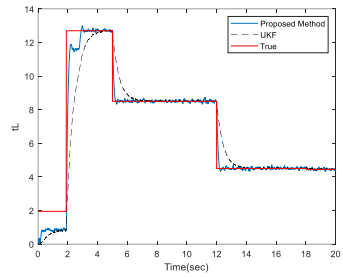

(a)

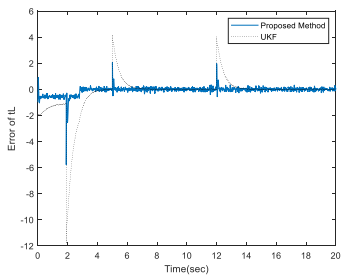

(b)

Fig. 7. a) Estimated load torque b) Load torque error

The trajectory of the estimated adhesion force (Fa) is determined by utilizing the estimated load torque data, denoted as $TL = 2rFa$. This information is extracted from the relevant section (1) and visually depicted in Fig.8.

To further evaluate the accuracy of the estimations provided by different approaches, the root mean square error (RMSE) for speed and load torque estimations is presented in Figs 9-10. These figures illustrate the RMSE obtained over 40 Monte Carlo runs. Fig 9 depict the RMSE of estimations over time, while Fig 10 display the mean and variance of the RMSE. Each bar in Fig 10 represents the mean and variance of the RMSE. The results indicate that the proposed method outperforms the Unscented Kalman Filter (UKF) in terms of both the mean and variance of the RMSE. The RMSE associated with the proposed method is consistently smaller than that of the other methods. This suggests that the speed and load torque estimated by the proposed method are closer to their actual values. Consequently, the adhesion force estimated using the proposed method is more accurate.

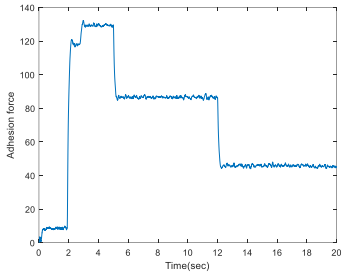

Fig. 8. Estimated adhesion force

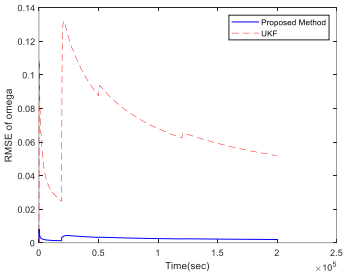

(a)

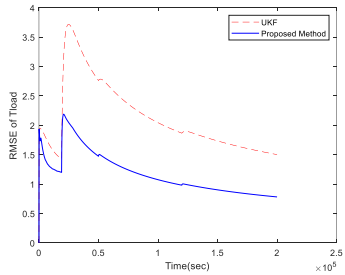

(b)

Fig. 9. RMSE over time (a) Omega (b) load torque

The comparisons presented in Table II include state-of-the-art methods, such as the approach proposed in [26], which addresses adhesion force estimation under dynamic and uncertain conditions. The results clearly demonstrate the superior accuracy and adaptability of the proposed method. Specifically, the proposed method exhibits strong performance in handling time-varying noise and

nonlinearities inherent in modern railway systems. This enhanced robustness, coupled with a competitive computational cost, highlights the practical advantages of the proposed method for real-time traction control applications.

The computational cost of the proposed method was evaluated through MATLAB simulations conducted on an Intel® Core™ i5-4590 CPU @ 3.3 GHz. The performance comparison of different algorithms is summarized in Table III. To clearly highlight the differences and facilitate a better understanding of the proposed method's efficiency, the computational costs are presented alongside the estimation accuracy metrics.

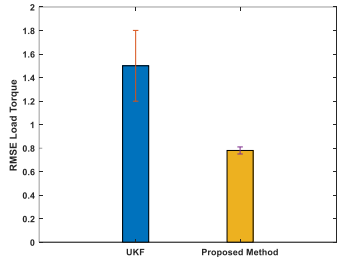

(a)

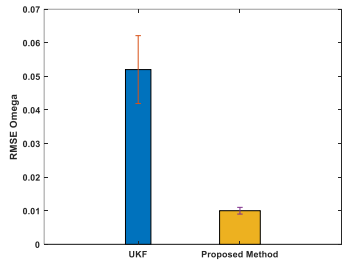

(b)

Fig. 10. RMSE (a) load torque (b) Omega

TABLE II Comparison of the Proposed Method with Recent Work

Method	Processing time (sec)
UKF	2.2
CKF[26]	2.1
Proposed Method	3.2

TABLE III Computational cost of algorithms

Method	RMSE	
	Omega	Load Torque
UKF	0.052	1.5
CKF[26]	0.041	1.2
Proposed Method	0.01	0.78

The results show that the running time of the proposed Intelligent SRCKF method is comparable to that of other state-of-the-art filters. Specifically, the proposed method requires approximately 1.1 seconds per run. However, this additional computational effort is justified by significant improvements in estimation performance, including a 20% reduction in speed RMSE and a 50% reduction in load torque RMSE. Moreover, the integration of DE for optimizing the noise covariance matrices ensures that the method remains feasible for real-time online operation. This balance between computational cost and enhanced accuracy confirms the practical applicability and superiority of the proposed approach for adhesion force estimation and induction motor parameter identification in industrial railway systems.

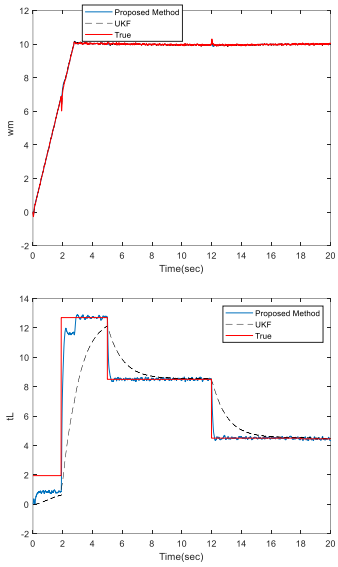

Fig. 11. Performance of EKF and proposed method under unknown statics noises

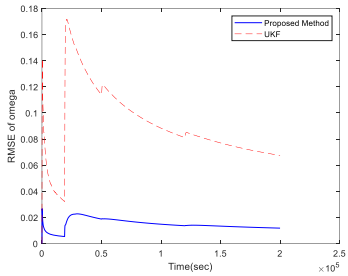

(a)

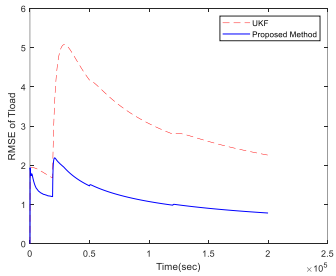

(b)

Fig. 12. RMSE over time (a) Omega (b) load torque

In order to assess the impact of unknown static noises on the estimation performance of our proposed method, we conducted a study. Specifically, we examined a scenario where process noise is mistakenly considered. In this

scenario, both our proposed method and the EKF method, which utilize the same R matrices, were simultaneously applied at high and low speeds. The estimation performances and errors of both algorithms were visualized in Fig.11. Upon analyzing the estimation performances at high and low speeds, it became evident that our proposed method outperforms the EKF method. This superiority can be attributed to the fact that the pre-determined Q matrix in the EKF method, determined through a trial-and-error approach, is not suitable for low and zero speeds. Consequently, it negatively affects the estimation performance of the EKF method. Furthermore, determining a Q matrix that consistently delivers satisfactory estimation performance across the entire speed range is challenging using the trial-and-error method. In contrast, our proposed method relies on the presumption that the noises are constrained to a specific energy level and does not necessitate any prior knowledge of these noises. Additionally, our method dynamically adjusts the process covariance, ensuring adaptability to varying conditions. The RMSE of speed and load torque estimations are presented in Figs 12-13.

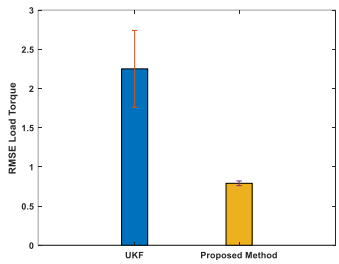

(a)

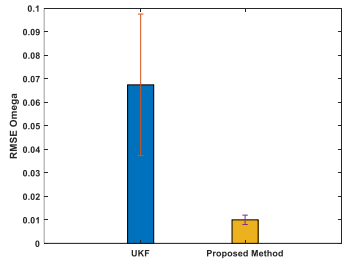

(b)

Fig. 13. RMSE (a) load torque (b) Omega

TABLE 2 Comparison of the Proposed Method with Recent Work

Method	RMSE	
	Omega	Load Torque
UKF	0.071	2.25
CKF[26]	0.053	1.99
Proposed Method	0.015	0.79

Fig 12 show the RMSE of estimations over time, while Fig 13 display the mean and variance of these RMSE values. It is evident that the proposed method outperforms the UKF in terms of both the mean and variance of the RMSE. Additionally, the RMSE of the proposed method is smaller than that of the UKF, indicating that the speed and load torque estimations by the proposed method are closer to their actual values. Consequently, the adhesion force estimated using proposed method is more accurate.

The comparisons presented in Table IV include state-of-the-art methods, such as the approach proposed in , which addresses adhesion force estimation under dynamic and uncertain conditions with unknown static noises. Similar to the previous case, the results clearly demonstrate the superior accuracy and adaptability of the proposed method. Specifically, the proposed ISRCKF exhibits strong performance in handling time-varying noise and nonlinearities inherent in modern railway systems. This enhanced robustness, coupled with a competitive computational cost, highlights the practical advantages of the proposed method for real-time traction control applications.

REFERENCES

[1] B.Chen; Z.Huang, W.Liu, R.Zhang,F.Zhou, J.Peng, "A Novel Adhesion Force Estimation for Railway Vehicles Using an Extended State Observer", IECON 2019 - 45th Annual Conference of the IEEE Industrial Electronics Society,2019.

[2] S.Shrestha, Q.Wu, & M.Spiryagin, "Review of adhesion estimation approaches for rail vehicles," International Journal of Rail Transportation, vol.7,no.2, 79-102,2019.

[3] A.Onat, & P.Voltr, "Velocity measurement-based friction estimation for railway vehicles running on adhesion limit: swarm intelligence-based multiple models approach," Journal of Intelligent Transportation Systems, 24(1), 93-107,2020.

[4] C.Schwarz,& A.Keck, " Simultaneous Estimation of Wheel-Rail Adhesion and Brake Friction Behaviour," IFAC-PapersOnLine, 53(2), 8470-8475,2020.

[5] S.Shrestha, M.Spiryagin, & Q.Wu, " Friction condition characterization for rail vehicle advanced braking system," Mechanical Systems and Signal Processing, 134, 106324,2019.

[6] Y. Liu et al., "Research on a lightweight rail surface condition identification method," *Applied Sciences*, vol. 15, no. 6, p. 3391, 2025.

[7] K. Zhao, P. Li, C. Zhang, J. He, Y. Li, and T. Yin, "Online accurate estimation of the wheel-rail adhesion coefficient and optimal adhesion antiskid control of heavy-haul electric locomotives based on asymmetric barrier lyapunov function," Journal of Sensors, vol. 2018, 2018.

[8] C. V. van de Merwe,J. D. Le Roux, "Estimation of Locomotive Adhesion Coefficients and Slip Ratios" , American Control Conference (ACC),2023.

[9] B.Leng,C.Tian,X.Hou,L.Xiong,W.Zhao,Z.Yu, "Tire-Road Peak Adhesion Coefficient Estimation Based on Multisource Information Assessment", IEEE Transactions on Intelligent Vehicles,vol.8,no.7,2023.

[10] Jing, H., Guangwei, L., Changfan, Z., et al.: "Maximum likelihood identification method for adhesion performance parameters of heavy duty locomotives", J. Electron. Meas. Instrum., 2017, vol.31, no.2, pp. 170–177.

[11] P. Pichlik and J. Zdenek, "Locomotive wheel slip control method based on an unscented kalman filter," IEEE Transactions on Vehicular Technology, vol. 67, no. 7, pp. 5730–5739, 2018.

[12] Hussain, I., Mei, T.X., and Jones, A.H., “Modeling and Estimation of Nonlinear Wheel-Rail Contact Mechanics”,Proceedings of Twentieth International Conference on System Engineering, pp. 219-223,Coventry, UK, 2009.

[13] T.X. Mei, and I. Hussain, “Detection of Wheel-Rail Contact Conditions for Improved Traction Control”, Proceedings of 4th International Conference on Railway Traction Systems, Birmingham, UK, 2010.

[14] I. Hussain, and T.X. Mei, “Multi Kalman Filtering Approach for Estimation of Wheel-Rail Contact Conditions”, Proceedings of the United Kingdom Automatic Control Conference, Coventry, UK, 2010.

[15] M. Wu and J. Zhou, "Wheel-Rail Adhesion Test Based on Full Scale Roller Rig," in Resilience and Sustainable Transportation Systems: Proceedings of the 13th Asia Pacific Transportation Development Conference, Shanghai, China, Jun. 2020, pp. 564–572.

[16] C. Wang a, L.B. Shi a, H.H. Ding a, W.J. Wang a, R. Ga las b, J. Guo a, Q.Y. Liu a, Z.R. Zhou a, M. Omasta b, “Adhesion and damage characteristics of wheel/rail using different mineral particles as adhesion enhancers”, Wear vol.477, 2021.

[17] I. Hussain, T. X. Mei, &, R. T. Ritchings , “Estimation of wheel-rail contact conditions and adhesion using the multiple model approach”, Vehicle System Dynamics,2013, vol.51,no.1,pp. 32–53, https://doi.org/10.1080/00423114.2012.708759

[18] J.Zhou, M.Wu, C.Tian, Z.Yuan, C.Chen , “Experimental investigation on wheel–rail adhesion characteristics under water and large sliding conditions”, Industrial Lubrication and Tribology, vol.73,no.2,2020.

[19] I. Hussain, “ Multiple Model Based Real Time Estimation of Wheel-Rail Contact Conditions”, PhD thesis, University of Salford,2012, http://usir.salford.ac.uk/id/eprint/38094.

[20] Y. Zhao,, B. Liang, & S.Iwnicki, “ Friction coefficient estimation using an unscented Kalman filter”, International Journal of Vehicle Mechanics and Mobility, vol.52,no. 1, pp.220–234,2014. https://doi.org/10.1080/00423114.2014.891757.

[21] R. Havangi and M. Moradi, “PSO-based EKF wheel–rail adhesion estimation,” *International Journal of Industrial Electronics, Control and Optimization (IECO)*, vol. 6, no. 1, pp. 49–62, 202.

[22] S. Sahl, E. Song, and D. Niu, "Robust Cubature Kalman Filter for Moving-Target Tracking with Missing Measurements," Sensors, vol. 24, no. 2, p. 392, Jan. 2024.

[23] Q. Chen, C. Yin, J. Zhou, Y. Wang, X. Wang, and, C. Chen, "Hybrid consensus-based cubature Kalman filtering for distributed state estimation in sensor networks," IEEE Sensors J., vol. 18, pp. 4561–4569, Jun. 2018.

[24] B. Gao, G. Hu, L. Zhang, Y. Zhong, and X. Zhu, "Cubature Kalman Filter with Closed-Loop Covariance Feedback Control for Integrated INS/GNSS Navigation," Chinese Journal of Aeronautics, vol. 36, no. 5, pp. 363–376, May 2023

[25] Q. Chen, J. Gong, X. Ge, S. Chen, and K. Wang, “Estimation of wheel-rail forces based on the STF-SCKF-NE algorithm,” *Measurement*, vol. 236, p. 114974, 2024.

[26] L. Quan, R. Chang, and C. Guo, “Vehicle state and road adhesion coefficient joint estimation based on high-order cubature Kalman algorithm,” *Applied Sciences*, vol. 13, no. 19, p. 10734, 2023.

[27] W. Wang, J. Fu, S. Bao, and X. Liu, “Vehicle state estimation using interacting multiple model based on square root cubature Kalman filter,” *Applied Sciences*, vol. 11, no. 22, p. 10772, 2021.

Ramazan Havangi is an Associate Professor of control systems with the Department of Electrical and Computer Engineering, University of Birjand, Birjand, Iran. His main research interests are inertial navigation, integrated navigation, estimation and filtering, evolutionary filtering, simultaneous localization and mapping, fuzzy, and soft computing.